

FATIGUE CRACK GROWTH RATES IN SIX PIPELINE STEELS *

A. Bussiba
NIST, Boulder, CO and
NRCN, Beer-Sheva, Israel

Ph. P. Darcis
NIST, Boulder, CO and
Gaithersburg, MD

J. D. McColskey, C. N. McCowan,
and T. A. Siewert,
NIST, Boulder, CO

G. Kohn
NIST, Boulder, CO and
NRCN, Beer-Sheva, Israel

R. Smith and J. Merritt
DOT/PHMSA
Washington D.C.

ABSTRACT

This study presents fatigue data for six different pipeline steels, with strengths ranging from Grade B to X100. A fatigue crack growth test for full thickness pipeline samples was developed using a Middle Tension (MT) type specimen. The six steels showed similar fatigue crack growth rate (da/dN) behavior. There were only minor differences among the steels for the threshold values and most of the stable crack growth regime. Larger differences were observed in the final stages of crack growth and fatigue failure. The effect of compressive residual stresses at the outer surface of the pipeline was also examined.

A Failure Assessment Diagram technique was used to evaluate the potential failures modes of the six pipeline steels, containing, as an example, an internal surface, semi-elliptic, axially oriented flaw. Mixed-mode failure was predicted for all of the steels.

INTRODUCTION

The rising demand for natural gas as an alternative energy source is motivating the construction of new pipelines. Considering this trend, the development of advanced steels with improved properties offers great advantages from the viewpoint of cost optimization (reducing wall pipe thickness, raising the operating pressure, lowering pipe laying costs and reducing welding costs) [1-4]. In addition, continuing efforts to develop enhanced methods may increase the availability, reliability, efficiency and safety of the pipeline life management process.

As the use of high-strength steels in severe conditions becomes more common, fitness-for-service assessments, which can be adopted at any stage in the life of a structure [5-7],

become more important in order to control fracture. During the concept and design phase, material properties are needed; key properties include the resistance to initiation and propagation of fatigue cracks, in terms of threshold, crack growth rate and critical stress intensity factor [8-10]. Fatigue cracks are known to be one of the damage mechanisms that occur during the service life of a pipeline. While fatigue is not often the ultimate cause of a failure, U.S. pipeline integrity management regulations require the characterization of such damage in susceptible types of pipeline materials.

The sources of the variable stresses that may initiate fatigue failure in a pipeline include fluctuation of the internal operating pressure, variation in external loads, temperature cycles and on-line compressor fluctuations. In addition, early damage, due to fatigue in transit, may initiate in-service fatigue cracking, which can be accelerated by an aggressive environment. Thus, by recognizing fatigue as a driving force in extending pre-existing defects or micro-cracks throughout service, the safety assessment of gas and oil pipelines must consider fatigue properties (and life predictions).

The current research program focuses on fatigue property comparisons between six different pipeline steels. The significance of fatigue crack growth for pipeline performance is explored using life prediction evaluations based on the Failure Assessment Diagram (FAD) [11]. The fatigue research utilizes linear-elastic fracture mechanics concepts (small crack-tip plasticity) that provide the basis for describing the phenomenon of fatigue crack propagation rate (FCPR). It is well accepted that the crack growth rate, da/dN (where a is the crack length and N the number of fatigue cycles), is controlled primarily by the stress intensity factor range, ΔK , and the most generally applicable law is the one suggested by Paris and Erdogan [12] in the form

* Contribution of an agency of the U.S. government, not subject to copyright

$$\frac{da}{dN} = C(\Delta K)^m, \quad (1)$$

where C and m are material constants. It has been shown by use of dimensional arguments that m must be a linear function of $\log C$. The dominant parameter is m , since it determines the ΔK dependence of the growth rate. The above expression adequately describes behavior for the mid range of da/dN , typically 10^{-5} mm/cycle to 10^{-3} mm/cycle. For lower growth rates, eq. (1) is found to be conservative, while for the higher growth rates it underestimates growth. Consequently, the entire fatigue curve has a sigmoidal shape for the crack growth rate with ΔK , as illustrated in Fig. 1 [13]. This curve is bounded by the fatigue critical stress intensity factor range, ΔK_{fc} , and the threshold, ΔK_{th} .

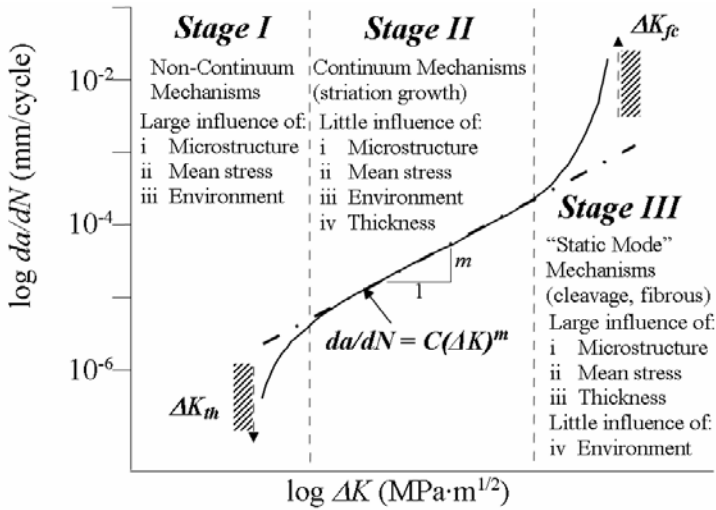


Figure 1. Primary mechanisms in steels associated with the three stages of fatigue crack growth. [13]

The second part of this paper applies the FAD (Fig. 2) (also called the R6 failure assessment diagram [7]) to assess the remaining pipeline strength and predict the residual life. This method is based on elastic-plastic fracture mechanics and describes the possible fracture modes (brittle to plastic collapse) of a pipeline containing a planar flaw for safety assessment.

In the FAD (level 2, as defined in the BS 7910 [11]), the critical confiscation (failure) is defined as:

$$K_r = \begin{cases} (1 - 0.14L_r^2) \left[0.3 + 0.7 \exp(-0.65L_r^6) \right] & L_r \leq L_{r(max)} \\ 0 & L_r > L_{r(max)} \end{cases}, \quad (2)$$

where $L_{r(max)}$ is determined by the type of pipe material. L_r and K_r are the load ratio and toughness ratio respectively.

L_r and K_r are calculated with use of the following equations:

$$L_r = \frac{\text{Applied load}}{\text{Collapse load}} = \frac{\sigma_{ref}}{\sigma_{0.2}}, \quad (3)$$

$$K_r = \frac{\text{Stress intensity factor}}{\text{Fracture toughness}} = \frac{K_I}{K_{mat}} = \frac{K_I^p + K_I^s}{K_{mat}} + \rho$$

where σ_{ref} is the reference stress, $\sigma_{0.2}$ the yield stress, K_{mat} the material toughness measured by stress intensity factor (SIF), K_I^p and K_I^s the applied stress intensity due to the primary stress distribution and the second stress distribution, respectively, and ρ the plasticity correction factor, given by eq. (4) [14].

$$\rho = \begin{cases} \rho_1 & L_r \leq 0.80 \\ 4\rho_1(1.05 - L_r) & 0.80 < L_r < 1.05 \\ 0 & 1.05 \leq L_r \end{cases}, \quad (4)$$

where

$$\rho_1 = 0.1 \left(\frac{\sigma^s L_r}{\sigma^p} \right)^{0.714} - 0.007 \left(\frac{\sigma^s L_r}{\sigma^p} \right)^2 + 0.00003 \left(\frac{\sigma^s L_r}{\sigma^p} \right)^5 \leq 0.25, \quad (5)$$

and σ^p and σ^s are the applied stresses due to the primary and the secondary stress distributions, respectively.

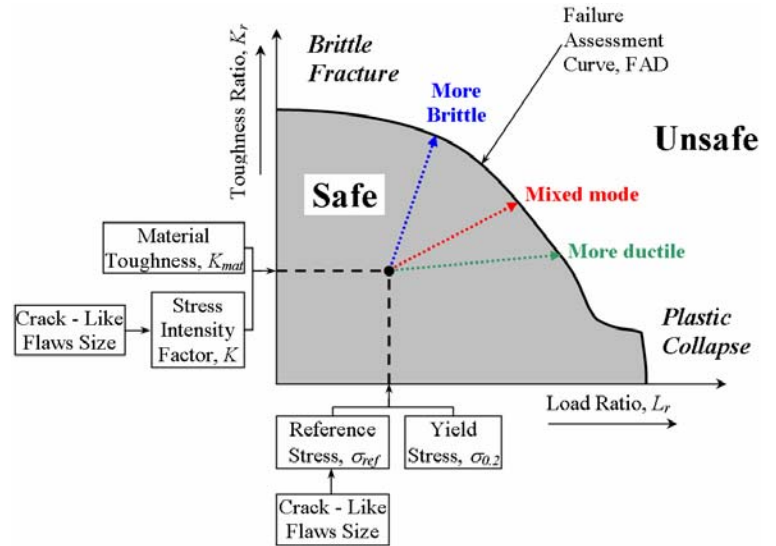


Figure 2. The failure locus for the strain hardening failure assessment diagram

MATERIALS AND EXPERIMENTAL PROCEDURES

Material properties

Six pipeline steels, including steel that had been in service on pipelines (used), were tested. The steels include five low-strength pipeline steels, # 1 to 5, and one high-strength pipeline steel, # 6. Table 1 summarizes the pipe dimensions.

Table 1. Designation of the tested steels

Steel #	1	2	3	4	5	6
Designation	N/A	X52	Grade B	N/A	N/A	X100
O. D. (inch)	20	20	22	20	22	52
O. D. (m)	0.51	0.51	0.52	0.51	0.52	1.32
Thickness (mm)	11.4	8.1	8.1	8.1	8.1	20.6
Remarks	Unused	Used	Used	Used	Used	Unused*

* pressure tested, but never put in service

Nominal chemical compositions of the selected steels are given in Table 2. As shown, steels No. 1 and 6 are characterized by low C, characteristic of more modern pipeline steels. Steel No. 1 has minor additions of Nb and V. The others steels contain higher C, as well P and S.

Table 2. Chemical composition of the tested steels (weight %)

Steel #	C	Mn	P	S	Si	Cr
1	0.06	1.46	0.01	<0.01	0.28	0.02
2	0.24	1.03	0.016	0.013	0.057	0.024
3	0.27	0.36	0.005	0.015	0.009	0.029
4	0.18	0.52	0.026	0.010	0.043	0.021
5	0.25	0.97	0.013	0.012	0.061	0.019
6	0.07	1.90	0.008	0.005	0.10	N/A

Steel #	Ni	Cu	V	Nb	Mo	Co
1	0.10	0.11	0.045	0.054	0.025	0.006
2	0.064	0.038	0.002	0.007	0.016	0.025
3	0.021	0.015	0.003	0.005	0.007	0.007
4	0.021	0.054	-	0.005	0.009	0.014
5	0.066	0.046	0.002	0.007	0.017	0.025
6	0.50	0.30	N/A	N/A	0.150	N/A

To measure the tensile properties of pipelines, flat tensile specimens were machined from pipeline steels # 1-5, and round tensile specimens (6 mm diameter) were machined from steel # 6. The flat specimens were full thickness. Those taken in a longitudinal orientation were 6 mm wide, and the transverse specimens were 3 mm thick. All specimens had a gauge length of 25.4 mm. Experiments were performed in a screw-driven tensile testing machine of 100 kN capacity, and a closed-loop servo-hydraulic machine of 100 kN capacity. Tests were conducted in displacement control at rates of 0.25 mm/min (for steels # 1-5) and 0.1 mm/min (for steel # 6). The differences in specimen shapes and displacement rates (*quasi-static*) are expected to have little effect on the mechanical properties. Two tests were conducted for the transverse (T) direction, and two for the longitudinal (L) direction, for each steel. The mean mechanical properties measured for the six steels are shown in Table 3; E is the Young's modulus, $\sigma_{0.2}$ the yield stress, σ_{UTS} the ultimate strength, e_u the uniform elongation, and e_f the fracture elongation.

Table 4 lists some measurements of the metallurgical features.

Table 3. Mechanical properties (mean)

Steel #	Orientation	E (GPa)	$\sigma_{0.2}$ (MPa)	σ_{UTS} (MPa)	$\sigma_{0.2}/\sigma_{UTS}$
1	L	211.1*	517	611	0.85
	T	N/A	543	606	0.90
2	L	211.1*	360	556	0.65
	T	N/A	448	576	0.78
3	L	212.1*	244	451	0.54
	T	N/A	255	459	0.56
4	L	210.6*	335	535	0.63
	T	N/A	428	560	0.76
5	L	213.8*	281	457	0.61
	T	N/A	250	454	0.55
6	L	N/A	694	801	0.87
	T	N/A	797	828	0.96

* Average of the dynamic elastic modulus

Steel #	Orientation	e_u	e_f	e_u/e_f
1	L	6.7 %	35.0 %	0.19
	T	8.0 %	27.4 %	0.29
2	L	12.3 %	32.7 %	0.38
	T	11.1 %	25.6 %	0.43
3	L	19.6 %	37.8 %	0.52
	T	18.8 %	38.0 %	0.49
4	L	12.9 %	34.9 %	0.37
	T	10.5 %	22.0 %	0.48
5	L	16.0 %	38.0 %	0.42
	T	19.5 %	35.0 %	0.56
6	L	4.3 %	25.0 %	0.17
	T	4.3 %	24.5 %	0.17

Table 4. Measurements (mean) of the metallurgical features

Steel #	1	2	3	4	5	6
Ferritic Grain Size (μm)	6.5	11.8	10.8	47.7	22.2	N/A
Pearlite Volume Fraction (%)	5	37.1	25.3	37.9	17.1	Bainite phase

Some of the steels had been in service for many years, and Young's modulus (calculated from the stress-strain curves) is subject to specimen effects such as surface irregularities and corrosion. *Dynamic elastic modulus measurements for the samples taken from the different pipeline steels # 1 - 5 were conducted according to standard ASTM E1876-01 [15].* Table 5 summarizes three dynamic elastic modulus measurements: $E(1)$, measured for out-of-plane flexure, which has the greatest strains on the wide, flat sides; $E(2)$, measured for in-plane flexure, which has the greatest strains on the long edges; and $E(3)$, measured for longitudinal vibrations with equal strains

across the cross section. For each steel, one dynamic elastic modulus test was conducted. The results show good correspondence between the steels, as might be expected.

Table 5. Three dynamic elastic modulus measurements

Steel #	1	2	3	4	5	6
$E(1)$ (GPa)	212.2	210.9	213.3	210.5	214.7	N/A
$E(2)$ (GPa)	210.0	212.8	211.5	211.5	214.7	N/A
$E(3)$ (GPa)	211.1	209.6	211.5	209.7	212.1	N/A

Figures 3(a) to 3(f) illustrate the microstructures of the various steels, which emphasize the following points:

- Steel # 1 is a ferrite-pearlite steel with low carbon (a low pearlite content) and a fine ferrite grain size (Fig. 3(a)). The surface is plastically deformed, presumably due to surface treatment prior to application of the coating to the pipeline (Fig. 3(a)).
- Steels # 2 (Fig. 3(b)) and # 4 (Fig. 3(d)) are characterized by a ferrite-pearlite banded structure.
- Steels # 3 (Fig. 3(c)) and # 5 (Fig. 3(e)) are ferrite-pearlite steels without banding.
- Steel # 6 is a ferrite-bainite steel [3] (Fig. 3(f)), with a small effective grain size and high dislocation densities compared with those of pearlite-ferrite steels (not measured).

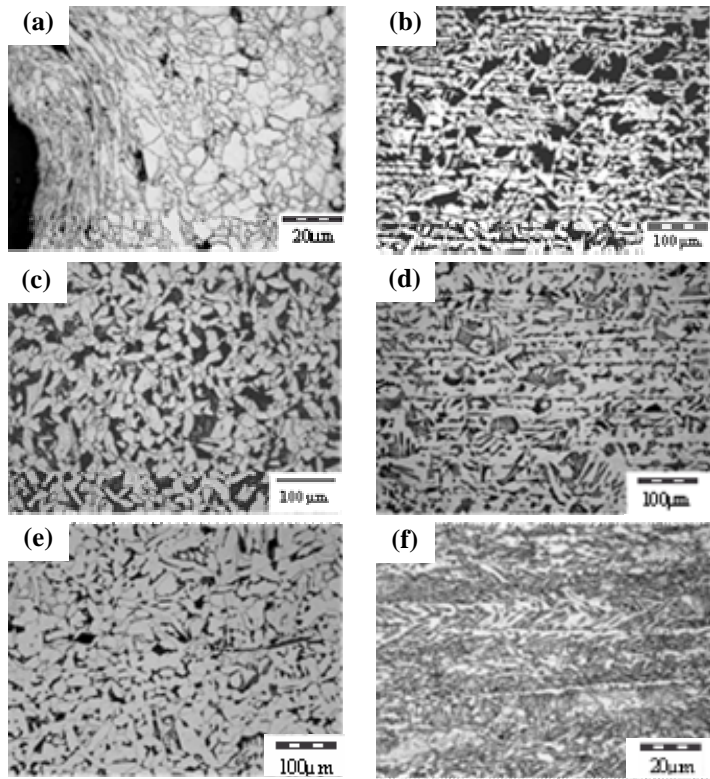


Figure 3. Microstructure of the selected steels (cross section parallel to the direction of rolling): (a) steel # 1, (b) steel # 2, (c) steel # 3, (d) steel # 4, (e) steel # 5, (f) steel # 6

Experimental set up

Fatigue tests were conducted on middle crack tension specimens (MT, as defined in ASTM E647-00 [16], middle crack tension) machined with longitudinal orientation, with respect to the pipe axis. With the exception of specimens from pipe #6, full thickness specimens were tested with no flattening. The samples from steel # 6 were too thick for the machine grip capacity and were mounted flat. Specimen geometry and dimensions are depicted in Fig. 4. A through-thickness notch with a tip radius of 0.1 mm was introduced by spark erosion. Due to the specimen curvature, special adapters were designed in order to allow application of a uniform pressure by the hydraulic grips without deforming the specimen. A special long-travel crack opening gauge (COG) was mounted directly across the notch opening for monitoring the crack length, a (Fig. 5). The standard equation for finding the crack length of an MT specimen from compliance data used a fourth-order polynomial. This standard equation is from ASTM E647-00 [16]. To achieve a better measurement of the compliance, the top and the bottom portions of the crack opening displacement (COD) vs. load curve were excluded, fitting only the interior points. This should prevent nonlinearities encountered from phenomena such as crack closure from affecting the slope of the curve. Furthermore, points are collected on both sides of the loading and unloading curve in order to average possible hysteresis effects.

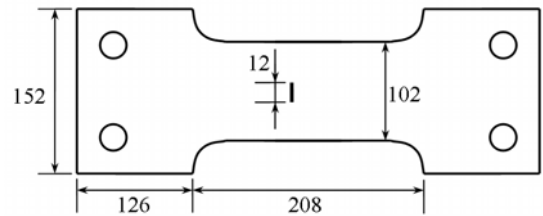


Figure 4. MT specimen dimensions (in mm)

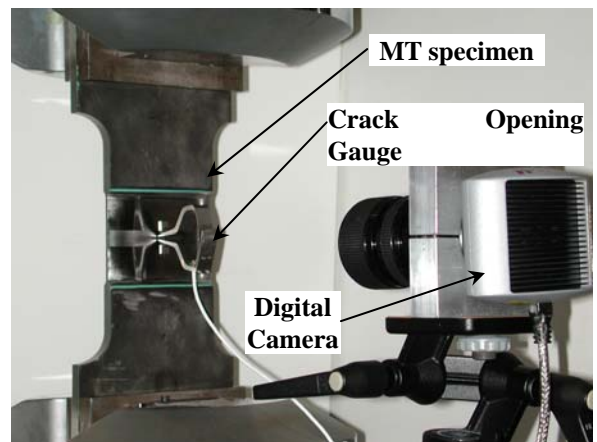


Figure 5. Experimental set up with COG location

The fatigue tests were conducted at room temperature with a computerized servo-hydraulic fatigue machine with a loading ratio, K_{min}/K_{max} , (where K_{min} and K_{max} are calculated from the

minimum and maximum applied load, respectively) equal to 0.4 at a frequency of 10 Hz.

Two tests were conducted on steel # 1 (11.4 mm thick); three on steel # 2 (8.1 mm thick); two on steel # 3 (8.1 mm thick); two on steel # 4 (8.1 mm thick); one on steel # 5 (8.1 mm thick) and two on steel # 6 (15.6 mm thick: flat specimens).

The stress intensity factor range, ΔK , was calculated according to the following equation [16]:

$$\Delta K = \frac{\Delta P}{B} \sqrt{\frac{\pi a}{W^2} \sec\left(\frac{\pi a}{W}\right)}, \quad (6)$$

where a is the half crack length, ΔP is the applied load range, and W and B are respectively the specimen width and thickness. This equation was used for uneven and flat specimens based on previous comparison results (private communication).

A stepwise increasing ΔK test was used following the Saxena equation [17] with a normalized K gradient (C) equal to 0.1 (1/mm). The initial ΔK was selected to be $6 \text{ MPa}\cdot\text{m}^{1/2}$. To minimize fatigue crack tip damage, the initial pre-cracking procedure was performed at a value of ΔK close to the actual testing value. The end test criterion was set to be a crack growth rate of $5 \cdot 10^{-2} \text{ mm/cycle}$.

EXPERIMENTAL RESULTS

The fatigue crack growth rate (FCGR) curves for the pipeline steels are illustrated in Figs. 6-9.

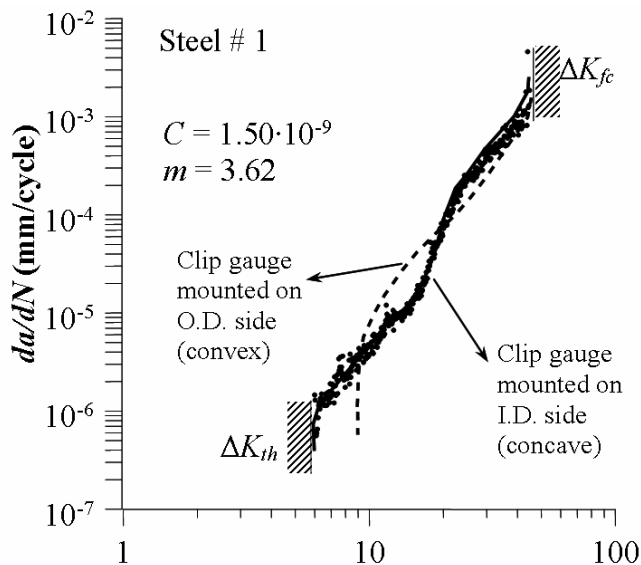


Figure 6. The effect of residual stresses at the O.D. side on the fatigue curve profile

Figure 6 emphasizes the effect of the residual stresses on the curve profile, presumably due to surface treatment (this residual stress field was not measured and not taken into account in the ΔK calculation). In the case where the COG was

mounted on the outer diameter (O.D.) side (convex), the crack opening was affected by the near-surface compressive residual stresses that influenced the COG reading, and made the apparent threshold value higher. However, once the propagating I.D. crack reached the location of the residual stresses, acceleration in the rate was observed. The opposite trend in the FCGR, namely a mirror image, was observed when the COG was mounted on the inner diameter (I.D.) side (concave).

Figure 7 compares the FCGR curves for the tested steels. There curves for the steels in stage I and stage II show similar trends. Minor differences are observed for the threshold value (see Fig. 8), which are excluded from the experimental initial ΔK value ($6 \text{ MPa}\cdot\text{m}^{1/2}$). In order to study the fatigue threshold, further tests with a K decreasing [16] need to be done (this is not the goal of the present study).

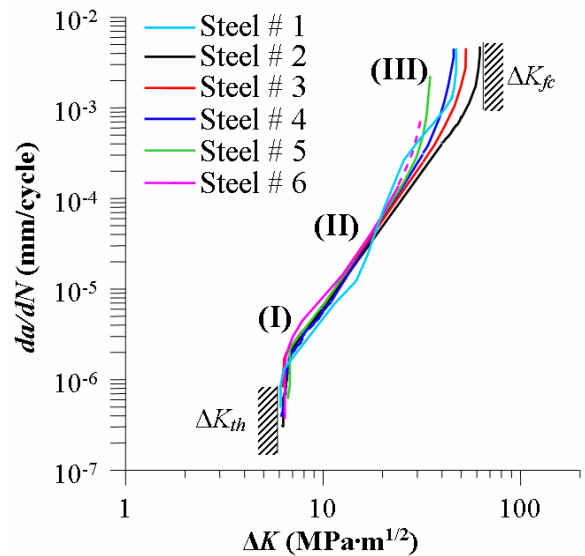


Figure 7. FCGR curves versus ΔK for the various steels

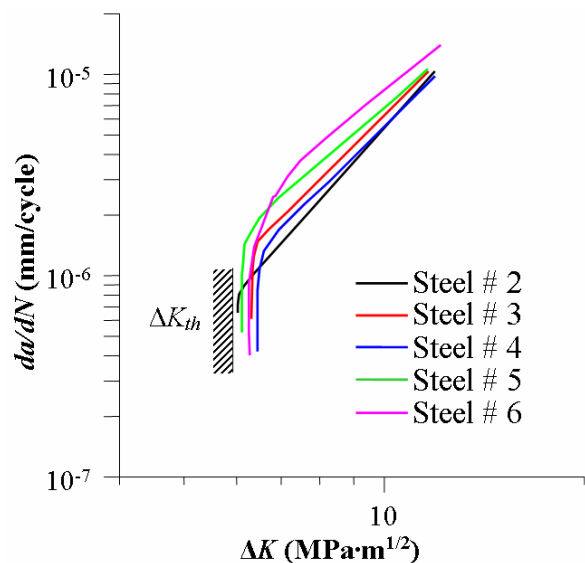


Figure 8. Expansion of the near threshold value regime

Near the end of stage II the FCGR curves begin to diverge slightly, and some differences develop between the steels in stage III, resulting in different ΔK_{fc} values. This behavior reflects the fact that failure mechanisms are influenced more than fatigue mechanisms by the microstructure of the steel in this higher loading regime and by the thickness of the specimen.

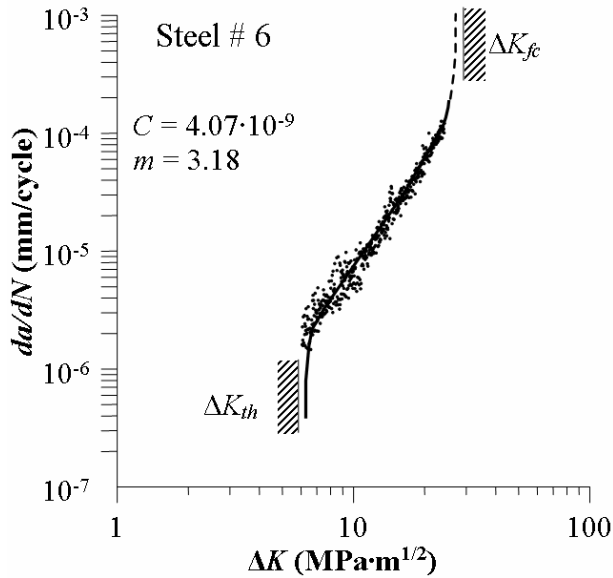


Figure 9. Sigmoidal type curve for steel # 6

The fatigue curve for the highest-strength steel (# 6) is shown in Fig. 9. The results in this figure are from two different fatigue tests (with loading ratio equal to 0.4). The data from the two tests are similar and group in a narrow band, defining the expected sigmoidal shape of the fatigue curve. The curve also shows the scatter of the FCGR data below a value of ΔK equal to $10 \text{ MPa}\cdot\text{m}^{1/2}$.

Table 6 summarizes the average FCGR results for the steels, and these data are used later to predict fatigue life for a sample with a flaw. In this table, the material toughness measured by stress intensity factor, K_{mat} (also defined by K_{Ic}), is calculated with the following equation:

$$K_{mat} = \frac{\Delta K_{fc}}{1-R}, \quad (7)$$

where R is the loading ratio (0.4). This equation is based on a fatigue test and further investigation needs to be done based on a fracture test in order to evaluate K_{mat} .

Table 6. Extreme values and Paris parameters (eq. 1)

Steel #	1	2	3	4	5	6
C^*	$1.50\cdot 10^{-9}$	$4.11\cdot 10^{-9}$	$2.30\cdot 10^{-9}$	$2.18\cdot 10^{-9}$	$2.53\cdot 10^{-9}$	$4.07\cdot 10^{-9}$
m	3.62	3.14	3.37	3.39	3.38	3.18
ΔK_{th}^{**}	6.1	6.3	6.1	6.5	6.1	6.2

K_{mat}^{**}	75	103	75	67	58	60
----------------	----	-----	----	----	----	----

* $\text{MPa}\cdot\text{m}^{1/2}$ & mm/cycle , ** $\text{MPa}\cdot\text{m}^{1/2}$, ΔK_{th} determined for $6\cdot 10^{-7} \text{ mm}/\text{cycle}$

From the statistical point of view, when the Paris law is used, m is fixed and C is the variable used to represent the scatter [18]. The distribution of $\ln(C)$ is assumed to be normally distributed (as the fatigue life is assumed lognormally distributed). Similar to the approach used in Risk Based Inspection (RBI), we make these assumptions to evaluate the scatter in the crack growth rate results. This approach is valid if the incremented estimates of C are independent.

In the stable crack growth region, a statistical study of the C parameter was conducted, assuming each of the FCGR test points were independent. The parameter m was taken as the mean value and the parameter C was calculated for each FCGR test point. Table 7 summarizes the statistical results for the steels (where S.D. is the standard deviation and N mean normal distribution). Figure 10 shows the scatter of the parameter C for steel # 6 to be random. Similar results were found for the other steels tested here, and this lack of a trend confirms the statistical independence of C .

Table 7. Statistical results for the steels

Steel #	$\ln(C)$	Mean C	Mean C + 2 S.D.	Number of points used
1	$N(-32.83 ; 0.33)$	$1.50\cdot 10^{-9}$	$2.89\cdot 10^{-9}$	770
2	$N(-30.16 ; 0.19)$	$4.11\cdot 10^{-9}$	$6.01\cdot 10^{-9}$	424
3	$N(-31.52 ; 0.19)$	$2.30\cdot 10^{-9}$	$3.37\cdot 10^{-9}$	396
4	$N(-31.66 ; 0.21)$	$2.18\cdot 10^{-9}$	$3.35\cdot 10^{-9}$	453
5	$N(-31.48 ; 0.19)$	$2.53\cdot 10^{-9}$	$3.67\cdot 10^{-9}$	245
6	$N(-30.31 ; 0.20)$	$4.07\cdot 10^{-9}$	$6.11\cdot 10^{-9}$	714

C in $\text{MPa}\cdot\text{m}^{1/2}$ & mm/cycle

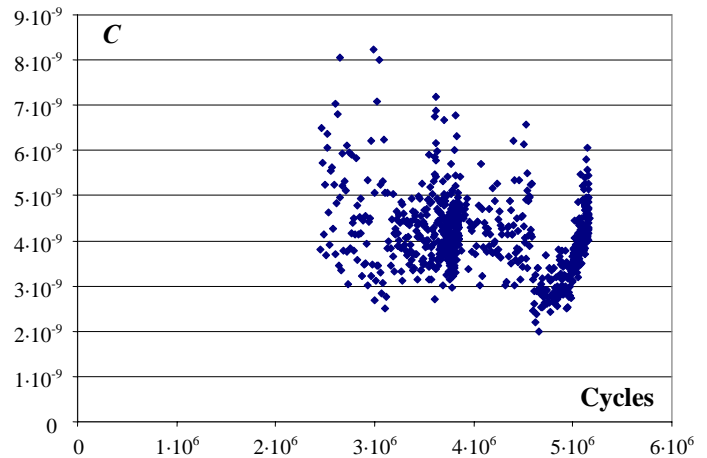


Figure 10. Scatter of the parameter C for steel # 6

These statistical results are similar to those of Johnston [19] ($m = 3$; $C = 5.85\cdot 10^{-9}$ and $C + 2 \text{ S.D.} = 9.49\cdot 10^{-9}$). This comparison is made because the mean plus two standard deviations (mean + 2 S.D.) given by Johnston coincides with

the upper bound PD 6493 [14], and because the BS 7910 [11] recommend a bilinear relationship.

The macro fatigue fracture surface for steels # 1 and 3 are shown in Fig. 11.

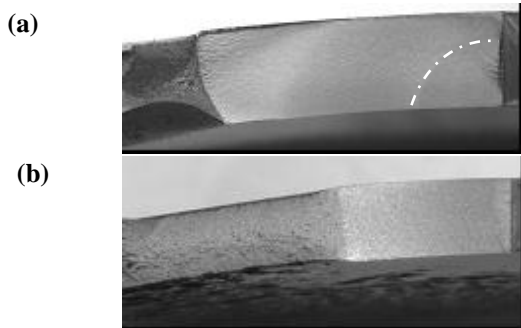


Figure 11. Macro fatigue fracture with different crack front profile: (a) asymmetric crack at the early growth in steel # 1, (b) symmetrical crack front obtained during the entire crack growth up to fracture in steel # 3

In Fig. 11(a) (steel #1), the asymmetric contour of the fatigue crack front (marked by a dashed line) developed due to the compressive residual stresses near the outer surface of the pipe. This abnormal crack front became more symmetric when the ligament near the outside surface of the pipe could not endure the loading level and the residual stresses became less effective. As the crack propagated and the stress intensity range approached the fatigue critical value, the crack front became straighter, with less curvature towards the outer diameter (O.D.) side (convex). In contrast, Fig. 11(b) shows a straight crack front. This front is typical for specimens with no plastic deformation on the surface, which is presumably due to a surface treatment (such as shot peening) done prior to coating a pipe. The effect of the residual stresses in steel # 1 is also reflected by the fatigue crack path. The crack propagates in a wavy manner on the O.D. surface (Fig. 12(a)), whereas at the I.D. surface of the crack path is more confined, with a tooth-like mode affected by the cross slip lines (Fig. 12(b)).

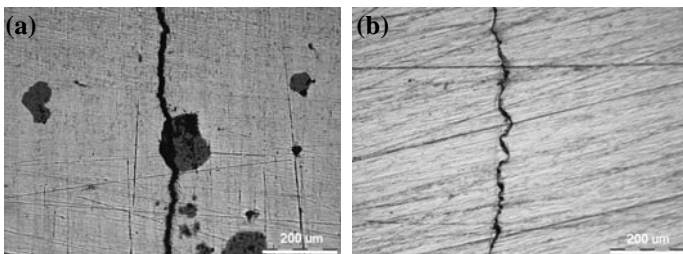


Figure 12. Fatigue crack profile at: (a) I.D. side $\Delta K = 11 \text{ MPa}\cdot\text{m}^{1/2}$, (b) O.D. side, $\Delta K = 10 \text{ MPa}\cdot\text{m}^{1/2}$

FATIGUE LIFE PREDICTION

The FAD technique, commonly used and defined in rules and recommendations [7,11,14], is a method for assessing the safety of pipelines containing planar flaws [20]. The approach is used here to provide examples of structural integrity predicted over the range in strength and fatigue properties of the six pipeline steels evaluated, assuming the presence of initial flaws. Results demonstrate flaw sizes that can be left as-is and so avoid unnecessary repairs. From the fatigue crack point of view, the crack growth can be managed until fracture (brittle fracture or plastic collapse, Fig. 2) occurs.

To illustrate the fatigue life prediction using the FAD, we assume an internal surface flaw in a cylinder, oriented axially (Fig. 13).

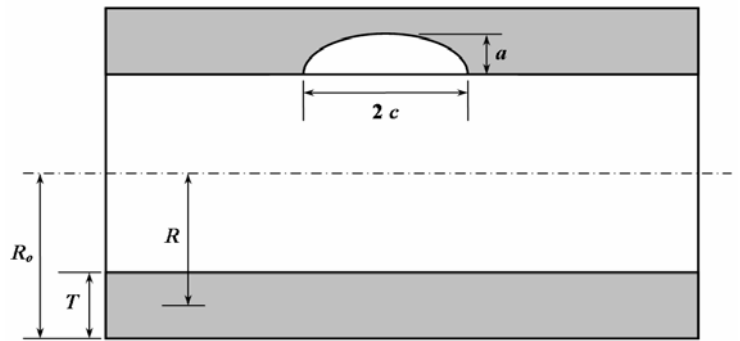


Figure 13. Axially oriented internal surface flaw in pipeline

We also assume that the pipelines are subjected to a uniform internal pressure, P , during their life and that they have the same dimensions. The focus is on predicting the range in service life characteristic of low and high strength steels both containing a flaw and having relatively small variations in fatigue crack growth rates.

Parameter selected

Parameters used to calculate a pipeline service-life were measured by the previous tests or are assumed. These parameters include:

- Pipeline dimensions: the steel # 6 (X100) pipeline dimensions were used for all the steels in this example; O.D. is 1.32 m and wall thickness is 20.6 mm (Table 1).
- Force, P : a loading waveform (sine wave), with a loading ratio of 0.4 (as used for fatigue the tests) and a maximum load of 6 MPa were used for these comparisons. This load was chosen to have a membrane stress below the yield stress of all six steels. For the lowest strength steel, the load was 76 % of the yield stress. This load was assumed to be the primary loading and not secondary loading, as the welding residual stresses, were assumed to be (eq. 3).
- Crack shape: axial direction and inner surface crack.
- Depth-length ratio, $a/2c$ (Fig. 13): a set value of 0.06 [20] is taken as an example.
- Initial crack depth (height): a length of 0.2 mm is assumed; this value is defined in order to have an initial stress

intensity factor range higher than the threshold ΔK_{th} (shown in Table 6). The choice of an initial crack length is not the purpose of the present work.

- Yield stress ($\sigma_{0.2}$): see Table 3.
- Ultimate strength (σ_{UTS}): see Table 3.
- Stress intensity factors: used to calculate the stress field in an internal surface flaw in a cylinder oriented axially. These factors are calculated from the following equation [21]:

$$K = Y \left(\frac{PR}{T} \right) \sqrt{\frac{\pi a}{Q}}, \quad (8)$$

where a is the crack depth of the surface flaw (Fig. 13), P the internal uniform pressure, T the pipeline thickness, R the mean radius (calculated from the outside diameter, R_o , and the thickness: $R = R_o - (T/2)$), Q the stress magnification factor, and Y the stress intensity factor correction. Q is equal to

$$Q = 1 + 4.593 \left(\frac{a}{2c} \right)^{1.65}, \quad (9)$$

and Y is equal to

$$Y = 1.12 + 0.053 \alpha + 0.0055 \alpha^2 + (1.0 + 0.02 \alpha - 0.0191 \alpha^2) \frac{\left(20 - \frac{R}{T} \right)^2}{1400}, \quad (10)$$

where α is equal to $(a/T)/(a/2c)$, and $2c$ is the crack length of the surface flaw (Fig. 13).

- Crack growth equation: used to calculate crack growth in depth direction. The Paris law (eq. 1) is used, with the parameters for each steel reported in Table 6.
- Material toughness measured by stress intensity factor, K_{fc} : see Table 6.
- Reference stress, σ_{ref} : this value was calculated with the following equation, from BS 7910 [11]:

$$\sigma_{ref} = 1.2 M_s P_m + \frac{2 P_b}{3(1 - \alpha'')^2}, \quad (11)$$

where P_m is the primary membrane stress ($P_m = (PR)/T$ is assumed, where P is the internal uniform pressure, T the pipeline thickness, R the mean radius), P_b the primary bending stress (no primary bending stresses were assumed: $P_b = 0$), α'' a function used to calculate the collapse stress, and M_s the stress magnification factor. M_s is equal to

$$M_s = \frac{1 - [a/(T M_T)]}{1 - (a/T)}, \quad (12)$$

where a is the crack depth of the surface flaw, T the thickness of the pipeline (Fig. 13), and M_T the stress magnification factor, equal to

$$M_T = \sqrt{1 + 1.6 \left(\frac{c^2}{(R_o - T)T} \right)}, \quad (13)$$

where c is the half length of the surface flaw and R_o is the internal pipeline radius (Fig. 13).

All these parameters were used with equations 1 to 5.

Fatigue life calculation and analysis

The FAD analyses were used to calculate the type of failure and the corresponding critical crack depth, a_c . The FCGR results were used to calculate the number of cycles needed to reach this critical crack size. Table 8 summarizes the results for each steel, and Fig. 14 shows the FAD analysis result for the X100 steel (# 6).

Table 8. Fatigue life calculation results, based on the FAD.

Steel #	Failure mode	Critical crack depth, a_c (mm)	a_c/T	Life duration (cycles)
1	More brittle	10.1	0.49	$1.63 \cdot 10^6$
2	Mixed mode	11.8	0.57	$1.38 \cdot 10^6$
3	More ductile	6.9	0.33	$1.61 \cdot 10^6$
4	More brittle	8.8	0.43	$1.68 \cdot 10^6$
5	Mixed mode	5.2	0.25	$1.46 \cdot 10^6$
6	More brittle	8.5	0.41	$1.30 \cdot 10^6$

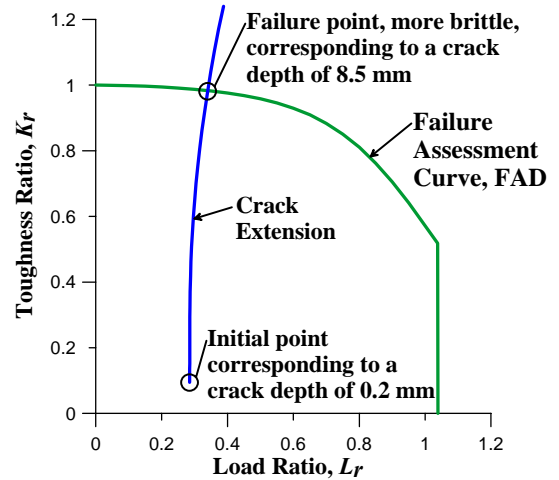


Figure 14. Failure Assessment Diagram for the X100 steel (# 6)

The results in Table 8 show the following:

- All of the steels were predicted to fail (pipeline leak) in a mixed mode, some more ductile and some more brittle. No obvious trends were seen.
- The critical crack depth, a_c , and the corresponding critical crack depth / pipeline thickness ratio criteria, a_c/T , are smaller for the lower strength steels (# 3 and # 5), because the initial membrane stress was closer to the yield stress. For the other steels, the ratio a_c/T is higher, between 0.4 and 0.6,

meaning that the crack can grow longer before reaching a critical size (Fig. 2).

- The higher-strength, more modern pipeline steels (# 1 and # 6) are predicted to have different life durations.

If a comparison is made for a crack growing from 0.7 mm and increasing up to a depth of 5.0 mm, results show no significant difference among the steels (Table 9). These example depths were chosen for their stable crack growth regions and to focus on the fatigue properties of the steels. The initial crack depth, 0.7 mm, with an initial da/dN higher than 10^{-6} mm/cycle, avoids any influence of stage I. The final crack depth, 5.0 mm, is reached before any critical crack depth steel failures (Table 8), thus avoiding of any influence of material toughness and plasticity in FAD analyses.

Table 9. Fatigue life calculated for a crack depth growing from 0.7 to 5 mm (mean and mean \pm 2 S.D.)

Steel #	1	2	3	4	5	6
Life duration (cycles)						
Mean - 2 S.D.	$2.19 \cdot 10^5$	$3.12 \cdot 10^5$	$3.26 \cdot 10^5$	$3.19 \cdot 10^5$	$2.98 \cdot 10^5$	$2.28 \cdot 10^5$
Mean	$4.22 \cdot 10^5$	$4.56 \cdot 10^5$	$4.77 \cdot 10^5$	$4.90 \cdot 10^5$	$4.32 \cdot 10^5$	$4.22 \cdot 10^5$
Mean + 2 S.D.	$8.14 \cdot 10^5$	$6.66 \cdot 10^5$	$6.97 \cdot 10^5$	$7.53 \cdot 10^5$	$6.27 \cdot 10^5$	$6.34 \cdot 10^5$

DISCUSSION

The fatigue properties of the six steels evaluated here represent three general groups of pipeline steels. The first group (steels # 2-5), represents ferrite-pearlite 0.2 to 0.3 carbon steels, which were used for many pipelines that are still in service today. The steels tested had significant differences in microstructure (grain size, pearlite content, banding), but show little difference in fatigue properties. This result is not surprising, particularly when the initiation and final stages of fatigue are not considered. The second group, the more modern, low-carbon, fine-grained ferrite-pearlite steel (# 1) had resistance to fatigue crack growth similar to that of the other ferrite-pearlite steels tested (group 1). The final group, representing the new higher-strength bainitic steels (# 6) had fatigue properties that compare well with those of the much lower strength ferrite-pearlite steels used in the past (groups 1 and 2). Considering the significant increase in strength made available to users of this steel, this is a good result (but should be confirmed with more testing).

The introduction of compressive residual stresses and distortion of the crystal structure at the conditioned surface (O.D.) influenced the initial stages of fatigue in samples from pipeline # 1. This result is not surprising. The resistance to fatigue damage in a component depends strongly on the properties of the surface and subsurface layers. This argument is substantiated when we compare the threshold values of

pipeline steel # 1 (Fig. 8) on the O.D and I.D. That for the O.D. side is almost $10 \text{ MPa}\cdot\text{m}^{1/2}$, whereas that for the I.D. side is nearly $6 \text{ MPa}\cdot\text{m}^{1/2}$. These trends were also reported by De Los Rios, et al. [22] on aerospace materials that had been subjected to shot peening. It has been stated that the surface treatment causes two main effects (delaying crack initiation and retarding the crack growth rate) that are responsible for these phenomena. First, the compressive residual stresses act as a closure stress on the crack, thereby increasing the resistance to crack opening; second, the strain hardening due to the locally deformed zone increases the resistance to the development of crack tip plasticity. So in practice, the application of such a treatment to the outer side of the pipeline can increase its resistance to fatigue crack initiation.

The association of the FAD with the FCGR data in the fatigue life assessment is able to take into account the fatigue properties, the mechanical properties and the failure mode of the steels. In our example, mixed-mode failures (some more ductile and some more brittle) were attained with the six steels considered here. The ferrite-pearlite 0.2 to 0.3 carbon steels (# 2-5) were predicted to have good service life, in spite of the small critical crack depth. Steels # 1 and # 6 were predicted to have slightly different lives, with the life for the higher strength steel (# 6) being the shorter. In this example, a more brittle failure mode was predicted for the X100 steel (# 6): however this more brittle mode corresponds to a leak in the pipeline. This predicted (through-thickness) fracture mode does not indicate the fracture mode for a crack in the axial direction on the pipe.

Both the FAD and FCGR analyses are based on stress intensity factors and could be incorrect if the linear-elastic fracture mechanics concept (small crack-tip plasticity) is invalid. In the case of significant plastic deformation near the crack tip, the use of elasto-plasticity methods such as the J-integral could be more relevant (such as the FAD level 3, in British Standard 7910, developed for ductile tearing assessment [11]). This could be the situation near the end of the fatigue life, close to fracture, as well as at any time during crack growth. FEM analysis could be helpful in the determination of the limit of the linear-elastic fracture mechanics applicability. Furthermore, the use of the Paris equation is inappropriate for the small crack growth observed in stage I, because of its nonlinearity. However, taking into account its limits, the combination of FCGR and FAD analyses appears to account for the main factors controlling pipeline fatigue life, and has in the past demonstrated reliable and conservative results [20].

CONCLUSIONS

The fatigue behavior of six pipeline steels was investigated. MT (full thickness) fatigue specimens were used, and were machined directly from the pipeline specimen along the axial orientation. Experimental results show minor differences in the threshold values of the steels, in stage I and for most of stage II. Some changes are observed for the fatigue

critical stress intensity factors for the steels in stage III. The ferrite-pearlite 0.2 to 0.3 carbon steels (# 2-5), the more modern low carbon ferrite-pearlite steel (# 1) and the new higher-strength bainitic steels (# 6) have similar fatigue properties, and these results are similar to those found in the literature [19].

Uncertainty in the fatigue crack growth rates was analyzed by attributing all the scatter in FCGR to the Paris law parameter C . The standard deviation of the C parameters was a substantial fraction of the mean values.

Residual stress effects on FCGR, between the I.D. and the O.D. were apparent for the sample from pipeline steel # 1. A significantly higher fatigue threshold due to the residual stress was observed. The introduction of compressive residual stresses at the outer surface of the pipeline affects the initiation stage.

The FAD technique was used as an example to relate the FCGR results to predicted pipeline performance. An internal surface, semi-elliptic, axially oriented flaw in a cylinder was assumed. Mixed-mode failure was predicted for all of the steels. Uncertainties in the fatigue crack growth rates produced significant standard deviations in the predicted lifetimes. Considering the uncertainties in the predicted range of lifetime, for example, the range between the mean value and the mean plus 2 standard deviations, the predicted lifetimes of all the steels tested are similar.

ACKNOWLEDGMENTS

The support of British Petroleum is gratefully acknowledged for providing the high-strength pipeline steel, and for the permission to publish this work.

The support of US Department of Transportation, Pipeline and Hazardous Materials Safety Administration, is appreciated.

The efforts of Dr Richard E. Ricker, Metallurgy Division, NIST, in conducting dynamic Young's modulus measurements on the pipeline steels are appreciated

REFERENCES

[1] JFE Steel Corporation - News Release - 2003 - 06/30, <http://www.jfe-steel.co.jp/en/release/2003/030630.html>.

[2] Nagahama, Y., and Yamamoto, S., 2003, "High Performance Steel Pipes and Tubes Securing and Exploiting the Future Demands", NKK Technical Review No. 88, pp. 81-87.

[3] Buzzichelli, G., and Anelli, E., 2002, "Present Status and Perspectives of European Research in the Field of Advanced Structural Steels", Proc. ISIJ International, 42 (12), pp. 1354-1363.

[4] Herman, J. C., 2000, "Thermo-mechanical Processing of Steels", Proc. IOM Communications, London, England, 585.

[5] ASME B31.G / Modified B31.G (RSTRENG), 1989, "Manual for determining the remaining strength of corroded pipelines", American Society of Mechanical Engineers.

[6] SINTAP, 1999, "Structural integrity procedures for European industry", Structural Integrity Procedure for Europe.

[7] Milne, I., Ainsworth, R. A., Dowling, A. R., Stewart, A. T., 1986, "Assessment of the Integrity of Structures Containing Defects", Document R/H/R6 - Revision 3, London: Central Electricity Generating Board.

[8] Vosikovsky, O., 1980, "Effects of stress ratio on fatigue crack growth rates in X70 pipeline steels in air and salt water", Journal of Testing and Evaluation, 8, pp. 68-73.

[9] Xiong, Q. R., Zhuang, C. J., Feng, Y. R., Ji, L. K., and Huo, C. Y., 1999, "Experimental studies on fatigue crack growth characteristics of 65 SSAW pipe", Proc. Fatigue 99, Beijing, China, pp. 1321-1326.

[10] Vosikovsky, O., 1975, "Fatigue crack growth in an X65 line-pipe steel at low cyclic frequencies in aqueous environments", Journal of Engineering Materials and Technology, pp. 298-304.

[11] British Standards Institution (BSI), BS 7910, 2005 "Guide to methods for assessing the acceptability of flaws in metallic structures", BSI, eds., London, England.

[12] Paris, P. C., and Erdogan, F., 1963, Journal Basic Engineering (Trans. ASME, D), 85, 528.

[13] Ritchie, R. O., 1977, "Influence of microstructure on near-threshold fatigue-crack propagation in ultra-high strength steel", Metal Science, pp. 368-381.

[14] PD 6493, 1991, "Guidance on Methods for Assessing the Acceptability of Flaws in Fusion Welded Structures", British Standard Institution, eds., London, England.

[15] ASTM Standard E1876-01, "Standard Test Method for Dynamic Young's Modulus, Shear Modulus, and Poisson's Ratio by Impulse Excitation of Vibration", 100 Barr Harbor Drive, ASTM Book of Standard Volumes 03.01, West Conshohocken, PA, 19428.

[16] ASTM Standard E647-00, "Standard Test Method for Measurement of Fatigue Crack Growth Rates", 100 Barr Harbor Drive, ASTM Book of Standard Volumes 03.01, West Conshohocken, PA, 19428.

[17] Saxena, A., Hudak, S. J., Donald, J. K., and Schmidt, D. W., 1978, Journal of Testing and Evaluation, 6 (3), p. 167.

[18] Darcis, Ph. P., Santarosa, D., Recho, N., and Lassen, T., 2004, "A fracture mechanics approach for the crack growth in welded joints with reference to BS 7910", Proc. 15th European Conference of Fracture, Stockholm, Sweden.

[19] Johnston, G. O., 1983, "Statistical scatter in fracture toughness and fatigue crack growth rates", ASTM STP 798: Probabilistic fracture mechanics and fatigue methods: application for structural design and maintenance, pp. 42-66.

[20] Jinheng, L., Xinwei, Z., Qingren, X., Chunyong, H., 2004, "Defective Pipeline Fatigue-Life Prediction Using Failure Assessment Diagram Technique", Proc. 5th International Pipeline Conference, paper No. 0487, Calgary, Alberta, Canada.

[21] ASME Boiler and Pressure Vessel Code, 1990, "Rules for In-service Inspection of Nuclear Power Plant Components", Section XI, American Society of Mechanical Engineers,

Appendix H, “Evaluation of Flaw in Ferritic Piping”, Addenda, eds..

[22] De Los Rios, E. R., Trull, M., and Leveres, A., 2000, “Extending the Fatigue Life of Aerospace Materials by Surface Engineering”, Proc. 13th European Conference of Fracture, M. Fuentes et al., eds., San Sebastian, Spain.